# Local structure of disordered Au-Cu and Au-Ag alloys

A. I. Frenkel,[1] V. Sh. Machavariani,[2] A. Rubshtein,[2] Yu. Rosenberg,[2,3] A. Voronel,[2] and E. A. Stern[4]

[1]*Materials Research Laboratory, University of Illinois at Urbana-Champaign, Urbana, Illinois*
*and Brookhaven National Laboratory, Building 510 E, Upton, New York 11973*

[2]*R. & B. Sackler School of Physics and Astronomy, Tel-Aviv University, Ramat-Aviv, 69978, Israel*

[3]*Wolfson Center for Materials Research, Tel-Aviv University, Ramat Aviv, 69978, Israel*

[4]*Department of Physics, Box 351560, University of Washington, Seattle, Washington 98195-1560*

(Received 17 May 2000)

X-ray-absorption fine structure (XAFS) and x-ray-diffraction (XRD) measurements of disordered alloys $Au_xCu_{1-x}$ and $Au_{0.5}Ag_{0.5}$ prepared by melt spinning were performed. In the $Au_{0.5}Ag_{0.5}$ alloy, no significant local deviations of the atoms from the average fcc lattice were detected while in $Au_xCu_{1-x}$ alloys, significant deviations of atoms from the average fcc lattice were found. Mean-square vibrations of the Cu-Cu distances revealed by the XAFS in $Au_xCu_{1-x}$ alloys indicate the weakening of contact between Cu atoms in the dilute limit. Our computer simulation for $Au_xCu_{1-x}$ clusters of $10^5$ atoms reproduces the main features of both the XAFS and XRD data.

## I. INTRODUCTION

As a result of our extended study of mixed ionic salts with atomic size mismatch: RbBr-KBr,[1,2] RbBr-RbCl,[1–3] and AgBr-AgCl,[4] strong deviations of the *local* structure from the *average* one were obtained using the x-ray-absorption fine-structure (XAFS) technique. In all the cases, equilibrium atomic positions were found to be shifted from the periodic crystalline sites, ascertained by x-ray diffraction (XRD). The structural refinement of XRD data as commonly done ignores the presence of local disorder and determines only the average periodic structure with the rms disorder about crystalline sites. XAFS is not biased against disordered contributions since it is sensitive to the local distribution of atoms (within 10 Å) around the absorbing atom. XAFS therefore solves the local structure with equal facility whether or not the actual structure is periodic. Interatomic distances, buckling angles (angular deviations of bonds from collinearity) and local compositions in mixed crystals were obtained using advanced methods of XAFS analysis (*ab initio* code FEFF6, Ref. 5 and data analysis package UWXAFS, Ref. 6).

Analysis of a mixed system of ionic salts $RbBr_xCl_{1-x}$ at concentrations $x$ throughout its full range has revealed a basic asymmetry between larger and smaller atoms' behavior:[3] the expansion of the shorter pair distance (Rb-Cl) with increasing concentration of Br is found to be greater than the contraction of the longer distance (Rb-Br) with increasing concentration of Cl. This asymmetry may be attributed to the difference between attractive and repulsive branches of interatomic pair potentials in these ionic salts and a qualitative explanation of local structure changes with concentration has been suggested.[3]

Recent XAFS study by Woicik, *et al.*[7] of bond-length distortions in bulk unstrained semiconductor alloys $Ga_{1-x}In_xAs$ with zinc-blende structure demonstrated that the distortions of the In-As and Ga-As bonds are equal, but opposite, within the uncertainties, in agreement with previous measurements by Mikkelson and Boyce.[8] For the same alloys epitaxially grown on different substrates, however, it was found that the

elastic strain induced a tetragonal distortion, splitting the bonds differently in different growth direction. In the diamond-based binary $Ge_xSi_{1-x}$ alloys strong compositional dependence (linear, within the experimental uncertainties) of Ge-Ge and Ge-Si bonds also has been recently measured.[9] The issue which has long remained unclear, whether Si-Si bond length exhibits the same compositional dependence as others, has been recently addressed by Aubry *et al.*[10] The authors obtained that the longer Ge-Ge bond length has stronger compositional dependence than that of the shorter Si-Si bond. The departure from the virtual crystal approximation (VCA) model also has been experimentally confirmed recently for the semiconductor alloys with wurzite structure.[11]

To understand whether the difference in bond lengths obtained for different systems with ionic (the case of mixed alkali and silver halide salts) and covalent (semiconductor alloys) bonds exists in the case of metallic bonds as well, we have prepared a series of disordered metallic alloys with large ($Au_xCu_{1-x}$) and small ($Au_xAg_{1-x}$) atomic size mismatch and analyzed their structure by both XAFS and XRD. A simple semiempirical computer simulation reproduces the distorted atomic structure in $Au_xCu_{1-x}$ determined by our experimental data.

The outline of the paper is the following. Details of the melt-spinning method of sample preparation, XRD and XAFS measurements are described in Sec. II. XAFS data analysis results are given in Sec. III. An algorithm and results of the computer simulation are briefly presented in Sec. IV. Discussion and conclusions are given in Secs. V and VI, respectively.

## II. EXPERIMENT

The series of disordered metallic alloys $Au_xCu_{1-x}$, which normally separate below 600 K, and $Au_{0.5}Ag_{0.5}$, which are miscible at all concentrations and temperatures, were prepared by the melt-spinning method. High purity Au (99.95%, Sigma, Israel) Ag, and Cu (both 99.99%, Holland-Israel Co.)

metals were initially melted together in vacuum in a quartz tube to form their respective alloys. Rapid quenching was achieved by pouring of a melt on a fast rotating copper drum. The estimated cooling rate was approximately $10^5$ K/sec. The compositions of our samples were established by energy dispersive x-ray spectroscopy in a scanning electron microscope.

XRD data were collected in the 30–120° 2Θ range with $CuK_\alpha$ radiation on the Θ:Θ powder diffractometer ''Scintag'' equipped with a liquid-nitrogen-cooled Ge solid-state detector. Peak positions and widths of Bragg reflections were determined by a self-consistent profile fitting technique with Pearson VII function.[12] Contributions of the $K_{\alpha2}$ radiation were subtracted from the total profiles, the obtained results correspond to only the $K_{\alpha1}$ component of $K_\alpha$ doublet. Lattice constant computation was carried out by reciprocal-lattice parameters refinement. The XRD analysis established the homogeneity of the alloys. No trace of phase separation or superstructure was observed for all the concentrations.

The condition $\Delta\mu x \lesssim 1$, where $x$ is the sample thickness and $\Delta\mu$ is the absorption edge step for Au $L_3$, Ag, or Cu $K$ edges, was used to calculate the proper thickness of the samples for the XAFS measurements. The obtained ribbons were thinned by rolling to the optimal thicknesses to avoid the sample thickness effect in XAFS.[13]

The XAFS measurements of Au $L_3$, Ag, and Cu $K$ edges were performed on beamline X11A at the National Synchrotron Light Source at 80 and 300 K (for $Au_xCu_{1-x}$ alloys) and at 10 and 300 K (for $Au_{0.5}Ag_{0.5}$ alloys) using a double crystal Si (111) monochromator. To eliminate the higher harmonics, the second crystal was detuned relative to the first one by 20% for Cu $K$-edge and by 15% for Au $L_3$-edge measurements. No detuning was found to be necessary for the Ag $K$-edge measurements. A Displex refrigerator was used for the low-temperature measurements.

## III. XAFS DATA ANALYSIS AND RESULTS

XAFS data were analyzed by the UWXAFS software.[6] The XAFS function $\chi(k)$ is given by

$$\chi(k) = \frac{\mu(k) - \mu_0(k)}{\Delta\mu(0)}, \quad (1)$$

where $k$ is the photoelectron wave number defined relative to the energy reference $E_0$ chosen in the middle of the absorption edge jump, $\Delta\mu(0)$ is the absorption edge jump, and $\mu_0(k)$ is a smooth atomic background. The AUTOBK code[14] was used to remove the background from the data. Statistical noise in the data measured at low temperature was very low, as illustrated in Fig. 1 which shows the $k$-weighted $\chi(k)$ obtained for two consecutive scans for both edges in $Au_{0.8}Cu_{0.2}$ at 80 K.

For a binary $A_xB_{1-x}$ alloy, the first nearest-neighbor (1NN) contributions to the XAFS signals measured at the $A$ and $B$ absorbing atoms can be written as

$$\chi^A(k) = y_{AA}\chi^{AA}(k) + y_{AB}\chi^{AB}(k),$$

$$\chi^B(k) = y_{BA}\chi^{BA}(k) + y_{BB}\chi^{BB}(k), \quad (2)$$
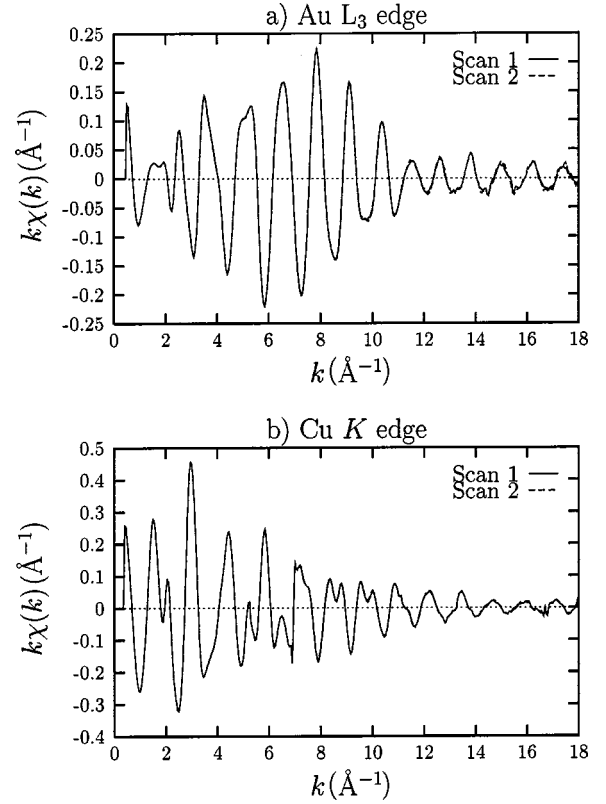


FIG. 1. $k$-weighted XAFS spectra of two consecutive scans of $Au_{0.8}Cu_{0.2}$ at 80 K for (a) Au $L_3$ and (b) Cu $K$ edges. Two minor monochromator-introduced glitches near $k=7.0$ and $16.5$ Å$^{-1}$ are visible in (b).

where $\chi^{ij}(k)$ are the partial contributions, weighted with $y^{ij}$, of the XAFS signals originating at a type-$i$ central atom surrounded by the type-$j$ neighbors only. The composition factor $y_{ij}$ is defined as the probability to encounter a type-$j$ atom as a 1NN to a type-$i$ central atom. Since for the first shell of atoms only single-scattering photoelectron contributions are important, each $\chi^{ij}$ [Eq. (2)] can be written as[15]

$$\chi^{ij}(k) = \frac{S_{0i}^2 N}{kR_{ij}^2} f_j(k) e^{-2k^2\sigma_{ij}^2} \sin[2kR_{ij} + \delta_{ij}(k)] e^{-2R_{ij}/\lambda_{ij}(k)},$$

$$(3)$$

where $S_{0i}^2$ is the passive electron reduction factor, $N$ is the number of atoms in a 1NN shell [$N=12$ for the fcc structure; the true number of $j$-type atoms in the 1NN shell is properly accounted for in Eq. (2) by having the $y_{ij}$ factor in front of $\chi^{ij}(k)$], $R_{ij}$ is the average interatomic distance between the $i$- and $j$-type atoms, $\sigma_{ij}^2$ is the mean-square relative disorder about $R_{ij}$, $f_j(k)$ and $\delta_{ij}(k)$ are the effective scattering amplitude and phase shift, respectively, and $\lambda_{ij}(k)$ is the photoelectron's mean free path. $f_j(k)$, $\delta_{ij}(k)$, and $\lambda_{ij}(k)$ were generated for all $i$-$j$ pairs using the FEFF6 code[5] for the fcc crystal structure model. XAFS analysis was performed concurrently for both edges for each concentration in each alloy while fitting the FEFF6 theory to data in $r$ space. $k^2$ weighting for $Au_{0.5}Ag_{0.5}$ and $k$ weighting for $Au_xCu_{1-x}$ have been applied to Fourier transform both data and theory to $r$ space. The excellent spatial resolution achieved in our experiment ($k_{max}=18–19$ Å$^{-1}$) allowed us to determine the character-

istics of the effective pair interaction potentials including anharmonic corrections at higher temperatures. In this paper, we discuss our results obtained from the low- and room-temperature measurements on $Au_xCu_{1-x}$ alloys only where our high data quality allowed an accurate evaluation of the characteristics of the effective pair interaction potentials between the atoms. We focus the discussion of temperature dependence in this article to the $Au_xCu_{1-x}$ alloys, as these show striking deviations from the fcc crystalline sites, in contrast to the $Au_xAg_{1-x}$ alloys.

The multiplicative factor $S_0^2$ can be often obtained directly from a fit of Eq. (3) to the data if the number of neighbors of a specific type is known in advance. In the case of disordered alloys, the situation is more complicated, since the partial coordination numbers for the pairs $AA$, $AB$, and $BB$ are unknown (although one can establish relationships between them, as it is shown below). Therefore an *a priori* knowledge of the $S_0^2$ factor is needed for the Cu $K$, Ag $K$, and Au $L_3$ edges. Because $S_0^2$ is a property of only the center atom, independent of its surroundings and temperature, these parameters were obtained by analyzing the temperature dependence of pure Au, Ag, and Cu metals XAFS data available at the University of Washington XAFS database, giving values of $S_0^2$ 0.88 for Au $L_3$ edge, 0.79 for Ag $K$ edge, and 0.94 for Cu $K$ edge. As a cross check of the values of $S_0^2$ we have used a procedure suggested by D. Koningsberger.[16] For each weighting factor $k$, $k^2$, and $k^3$, used in the Fourier transform, the value of $S_0^2$ was varied between 0.7 and 1.0 (the typical range of reasonable values for $S_0^2$) with a 0.05 increment and $\sigma^2$ for the first 1NN bonds was obtained from the best fit. Then $\sigma^2$ was plotted as a function of $S_0^2$ for each weighting factor. The three curves intersect at almost the same point providing the optimal values of both $S_0^2$ and $\sigma^2$. The $S_0^2$ values so obtained were in good agreement with those determined from the pure materials and the $\sigma^2$ so obtained agreed well with those determined from the temperature dependence.

In our fitting procedure, we varied the 1NN pair $R_{ij}$ and the $\sigma_{ij}^2$ independently for the homometallic pairs $A$-$A$ and $B$-$B$. The pair $R_{AB}$ and the $\sigma_{AB}^2$ of the heterometallic $A$-$B$ pair were constrained to be the same as analyzed from each edge XAFS data, as they must. The local composition factor $y_{AA}$ of $A$-$A$ pairs was allowed to vary in order to account for the possible short-range order. The following obvious constraints were applied to relate the composition factors $y_{AB}$, $y_{BA}$, $y_{BB}$, and $y_{AA}$, therefore reducing the number of fitting parameters:

$$y_{AB} + y_{AA} = 1,$$

$$y_{BB} + y_{BA} = 1. \qquad (4)$$

The composition factors of the heterometallic pairs $y_{AB}$ and $y_{BA}$ are related to one another through the macroscopic concentrations $x_A$ and $x_B$ of the alloy components[17] by

$$y_{AB} = \frac{x_B}{x_A} y_{BA}. \qquad (5)$$

For the $Au_{0.5}Ag_{0.5}$ alloys, the fits were refined for the Au and Ag edges concurrently, for data measured at 10 and 300

K. For the $Au_xCu_{1-x}$ alloys, the refinement was performed for the Au and Cu edges concurrently, for data measured at 80 and 300 K. For comparison, the XAFS data of pure Au, Ag, and Cu metal foils available in the XAFS database in the University of Washington,[18] collected at 80 and 300 K were also analyzed. For all the data, the corrections $\Delta E_0^{Au}$, $\Delta E_0^{Ag}$, $\Delta E_0^{Cu}$, to the arbitrarily chosen photoelectron energy origins were varied in the fits for Au, Ag and Cu central atoms, respectively.

If static structural distortions are present, the mean-square deviation $\sigma^2$ of the 1NN distance may be presented as a superposition of a static $\sigma_s^2$ and dynamic $\sigma_d^2$ terms:

$$\sigma^2 = \langle (r - \langle r \rangle)^2 \rangle = \sigma_s^2 + \sigma_d^2. \qquad (6)$$

To separate the temperature-independent $\sigma_s^2$ and temperature-dependent $\sigma_d^2$, one can use a simple correlated Einstein model[19] for $\sigma_d^2$:

$$\sigma_d^2 = \frac{\hbar}{2\omega\mu} \frac{1 + \exp(-\Theta_E/T)}{1 - \exp(-\Theta_E/T)}, \qquad (7)$$

where $\omega$ is a bond vibration frequency, $\mu$ is the reduced mass of the pair, and $\Theta_E = \hbar\omega/k_B$ is the Einstein temperature. Thus the total $\sigma^2(T)$ in this approximation depends on $T$ and two parameters only: $\omega$ and $\sigma_s^2$. By concurrent refinement of the XAFS data at two temperatures (80 and 300 K) one can solve Eqs. (6) and (7) for $\sigma_s^2$ and $\omega$.

The 1NN shell fits to the Au $L_3$ and Ag $K$ XAFS in $Au_{0.5}Ag_{0.5}$ at 10 K, and to the Au $L_3$ and Cu $K$ XAFS in $Au_{0.8}Cu_{0.2}$ data at 80 K are shown in Figs. 2 and 3, respectively.

Au-Au, Au-Ag, and Ag-Ag bond lengths obtained in the $Au_{0.5}Ag_{0.5}$ alloy and in the Au and Ag metals from the low- and room-temperature XAFS measurements are summarized in Table I. The temperature-dependent fits are consistent with $\sigma_s^2 = 0$. This is not surprising since the changes in $R_{ij}$ are small as a function of concentration in the Au-Ag alloy system, and, as discussed below, the structure does not have significant deviations from the crystalline fcc structures. To compare the disorder in the 1NN bond lengths in the $Au_{0.5}Ag_{0.5}$ alloy measured at 10 K with that measured in pure metals at 80 K, we used Eq. (7) and obtained values of Einstein temperatures for each bond to calculate $\sigma^2$ at 80 K in the alloy. The values of $\sigma^2$ obtained for these bonds at 80 K are given in Table II.

The fit of the $Au_{0.5}Ag_{0.5}$ sample at 10 K found that the 1NN $y_{Au-Au}$ is 0.45(1), and thus $y_{Au-Ag}$ from Eq. (4), is 0.55(1), indicating some short-range ordering from a random distribution of $y_{Au-Ag} = y_{Au-Au} = 0.5$. The short-range-order (SRO) parameter, defined as

$$\alpha = 1 - \frac{y_{AB}}{x_B}, \qquad (8)$$

is then equal to $-0.10(2)$, in good agreement with previously reported values of $-0.08$ (Ref. 21) and $-0.10$ (Ref. 22) obtained by diffuse x-ray scattering measurements. By contrast, in the $Au_xCu_{1-x}$ alloys, the 1NN compositions
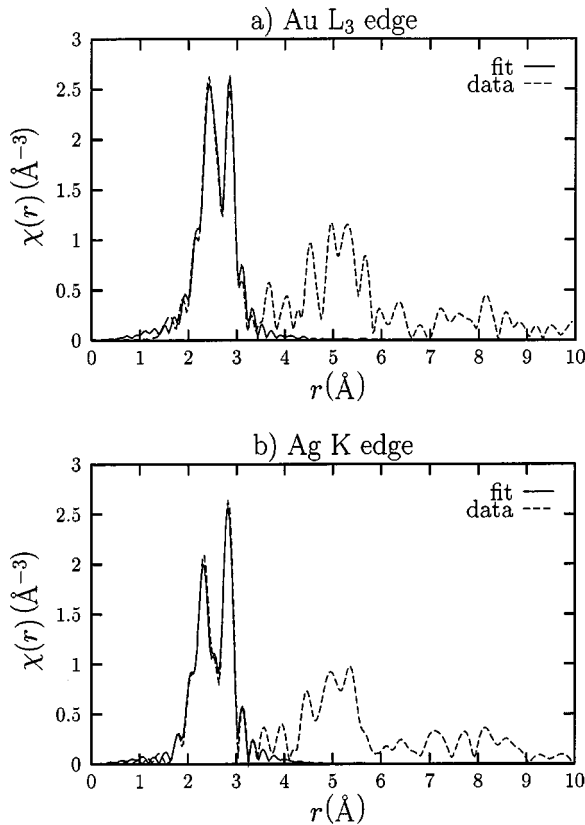
FIG. 2. Fourier transforms of the $k^2$-weighted XAFS spectra concurrently fitted with FEFF6 theory (solid) to the data (dash) of $Au_{0.5}Ag_{0.5}$ at 10 K for (a) Au $L_3$ and (b) Ag $K$ edges.



FIG. 3. Fourier transforms of the $k$-weighted XAFS spectra concurrently fitted with FEFF6 theory (solid) to the data (dash) of $Au_{0.8}Cu_{0.2}$ at 80 K for (a) Au $L_3$ and (b) Cu $K$ edges.

$y_{Au-Au} = x$ within 1%, consistent with no SRO in the alloys for all concentrations measured, and thus indicating a random distribution of atoms.

Figure 4(a) shows 1NN distances for Cu-Cu (triangles), Cu-Au (squares), and Au-Au (circles) atomic pairs. One can see the clear difference between these pairs similar to what was observed previously for the mixed salts $RbBr_xCl_{1-x}$ (Ref. 3), namely, the shortened Au-Au distances vary less than do the elongated Cu-Cu ones. As discussed in Ref. 3, such an asymmetry is caused by the stronger short-range repulsive forces compared to the longer range attractive forces of the interatomic potential.

The difference in behavior of the Au-Au and Cu-Cu pairs with concentration reveals itself even more clearly in the results of $\sigma^2$ measurements [Fig. 4(b)] published in our previous conference report.[23] While the $\sigma^2$ of the Au-Au pairs does not change strongly with concentration (which is consistent with a relatively small decrease in Au-Au pair length with respect to its value in pure Au), the $\sigma^2$ for the Cu-Cu pairs increases drastically. This is consistent with the weakening of the Cu-Cu force constant as the smaller Cu atoms become further apart at larger concentrations of Au, while both the Cu-Au and Au-Au 1NN pairs remain in contact sensing the repulsive force at all concentrations.

Table III presents the $\sigma_s^2$ determined from the temperature variation for several concentrations (only those values where the results are significantly larger than their error bars). At the high concentration of Au the data on the Cu-Cu pairs are not conclusive to make a decision in favor of predominantly dynamic or static disorder. Therefore the question of whether
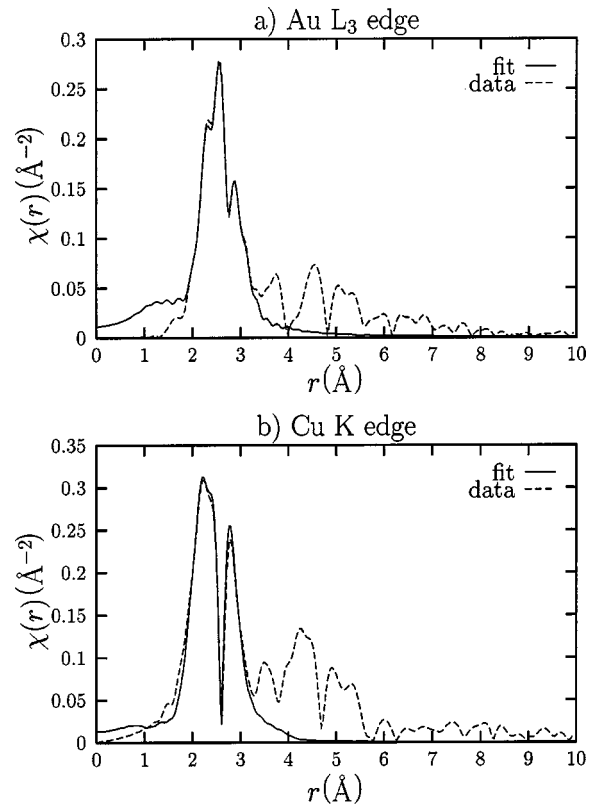
the large Cu-Cu atomic disorder around $x=0.8$ is predominantly a dynamic one with large vibrational amplitude, or a static one, is not directly determined from our data. However, extrapolating the lower $x$ dependence to 0.8 suggests that the large disorder there is predominantly static. Finally, the results of the XRD measurements on the same $Au_xCu_{1-x}$ alloys are plotted in Fig. 5, as deviations from the linear Vegard's law.

## IV. COMPUTER SIMULATION

The knowledge of the structure of mixed crystals may be enriched further if the information obtained from the two complementary techniques, XRD and XAFS, is visualized by a computer simulation. The fcc lattice with lattice parameter $a$ was randomly populated by Cu and Au atoms as per the concentration of the alloy. A single interatomic interaction between Au-Au 1NN atoms was fit to XAFS measurements on both the pure metal and the alloys, and similarly for the Cu-Cu 1NN atoms. Both 6-12 and 6-18 Lennard-Jones potentials were tried in the fit but only the 6-18 potential could give a reasonable fit to the experimentally determined lattice parameters at all concentrations, as described below. Since both pairs of atoms' 1NN distances change significantly in the alloying [Fig. 4(a)], the anharmonic behavior of the potentials have to be matched to the alloy XAFS results and our fit indicates that the larger anharmonicity of the 6-18 potential does this better.

The total potential energy taking into account pair interactions between the nearest-neighbor atoms only is $U$

TABLE I. First nearest-neighbor (1NN) bond lengths (in Å) in $Au_{0.5}Ag_{0.5}$ alloy and pure Au and Ag metals, and the average 1NN distance determined from x-ray diffraction (Ref. 20) and XAFS at low (LT) and room (RT) temperatures. LT measurements were performed at 10 K for the alloy and 80 K for pure metals.

| $x_{Au}$ | $T$ | Ag-Ag | | Au-Au | | Ag-Au | | $\langle R_{1NN}\rangle$ | |
|---|---|---|---|---|---|---|---|---|---|
| | | XRD | XAFS | XRD | XAFS | XRD | XAFS | XRD | XAFS |
| 0 | LT | 2.878 | 2.882(5) | | | | | 2.878 | 2.882(5) |
| 0 | RT | 2.889 | 2.88(1) | | | | | 2.889 | 2.88(1) |
| 1 | LT | | | 2.876 | 2.876(5) | | | 2.876 | 2.876(5) |
| 1 | RT | | | 2.884 | 2.89(1) | | | 2.884 | 2.89(1) |
| 0.5 | LT | | 2.875(5) | | 2.869(2) | | 2.874(2) | 2.873 | 2.873(3) |
| 0.5 | RT | | 2.89(2) | | 2.891(6) | | 2.879(4) | 2.881 | 2.88(1) |

$=\Sigma' V_{T_i T_j}(|\vec{r}_i-\vec{r}_j|)$, where $T_i$ is the type of the atom in the $i$th site, i.e., $A$ or $B$, the summation is over nearest neighbors only. The 6-18 Lennard-Jones potential for $V_{T'T}$ is chosen in the form which makes it convenient for further interpretation:

$$V_{T'T}(r)=\frac{K_{T'T}R_{T'T}^2}{216}\left[\left(\frac{R_{T'T}}{r}\right)^{18}-3\left(\frac{R_{T'T}}{r}\right)^6+2\right], \quad (9)$$

where the parameter $K_{T'T}$ is a force constant at $R_{T'T}$, the equilibrium bond length of the $T'$-$T$ atomic pair. The constant 2 in the right side of Eq. (9) is added to shift the energy scale to zero at the equilibrium position (instead of the usual presentation with zero energy at the infinite interatomic distance). In such a presentation the potential energy of a free equilibrated pair $V_{T'T}(R_{T'T})$ equals to zero and the total potential energy of the cluster corresponds to the deviation of the energy of the disordered crystal from the energy of two separated phases, i.e., it is a measure of the instability or stability of the alloy.

$R_{Au-Au}$ and $R_{Cu-Cu}$ are determined from the lattice parameters $a_{Au}$ and $a_{Cu}$ of the pure Au and Cu: $R_{Au-Au}=a_{Au}/\sqrt{2}$ and $R_{Cu-Cu}=a_{Cu}/\sqrt{2}$. Force constants $K_{Au-Au}$ and $K_{Cu-Cu}$ are determined from the temperature dependence of $\sigma^2$ for pure Au and Cu [Eq. (7)]. The two values $R_{Au-Cu}$ and $K_{Au-Cu}$ were used as fitting parameters. All the six parameters $K_{T'T}$ and $R_{T'T}$ are assumed to be concentration independent (see Table IV).

We performed a minimization of the total potential energy of a cluster of $10^5$ atoms while locally distorting both Au and Cu atoms from their ideal fcc lattice positions. To find the equilibrium positions for $N$ atoms in a cluster, i.e., to find a minimum of the total potential energy, we used the following iterative procedure. First, we fixed the positions of all but the $i$th atom and minimized the total potential energy as a function of the position of $i$th atom only. This resulted in the first approximation for the equilibrium position of the $i$th atom. After the $i$th atom was fixed in its new position, this procedure was repeated to the rest of the atoms in the cluster. A series of iterations were performed until the ratio $\Delta U/U$ becomes smaller than $10^{-4}$, where $\Delta U$ is an estimated maximal possible error, $\Delta U=NF_{max}^2/K_{eff}$, $F_{max}$ is a maximal force (among all the atoms of the cluster) acting on the atoms, $K_{eff}$ is an average effective force constant of the pairs.

Next, the equilibrium atomic positions and the total energy $U$ of the cluster were calculated as a function of the

lattice parameter $a$. The lattice parameter $a_0$ which corresponds to the minimum of $U(a)$ was then compared with the experimental result (see Fig. 5). The symbols in Fig. 5 correspond to our XRD data, the solid curve presents the result of the $a_0$ calculation. The Cu-Cu, Cu-Au, and Au-Au pair distances were obtained by averaging over the cluster with the lattice parameter $a_0$. They are presented in Fig. 4(a) (solid, dashed, and dotted curves, respectively). In our calculations the number of atoms $N$ is 108 000, i.e., the simulation box contains $30\times30\times30$ fcc unit cells with four atoms per one cell. To ensure that the calculation presents only the bulk effect (which is important for comparison with XAFS data), i.e., to minimize the influence of fixed boundaries on our numerical results, we display the results in the figures obtained from the inner atoms which are separated from the cluster surface by at least two layers.

Figures 4 and 5 demonstrate the compatibility of our cluster model with both the XAFS and XRD experimental data. The fact that only two additional fitting parameters ($R_{Cu-Au}$ and $K_{Cu-Au}$) beyond the ones found from the pure metals are necessary to describe the main features of the mixed alloy structure shows the reasonability of our model for describing the Au-Cu alloy. The results of our computer simulation are rather close to the Monte Carlo simulation[24] and *ab initio* calculation of the quasirandomly structured alloy.[25] Moreover, our simulation better fits the experimental data. The inner part ($3\times3\times3$ unit cells) of the $Au_{0.5}Cu_{0.5}$ cluster obtained from computer simulations is visualized in Fig. 6.

## V. DISCUSSION

The detailed structure of the disordered $Au_xCu_{1-x}$ alloys was investigated by XAFS, XRD, and computer simulation. The atoms were found to be randomly disordered among the atomic sites which deviated locally from the average fcc crystal sites. Particularly interesting is the profoundly differ-

TABLE II. Mean-square deviations (in $Å^2$) in 1NN pair lengths determined from XAFS data of $Au_{0.5}Ag_{0.5}$ alloy and pure Au and Ag metals at 80 K.

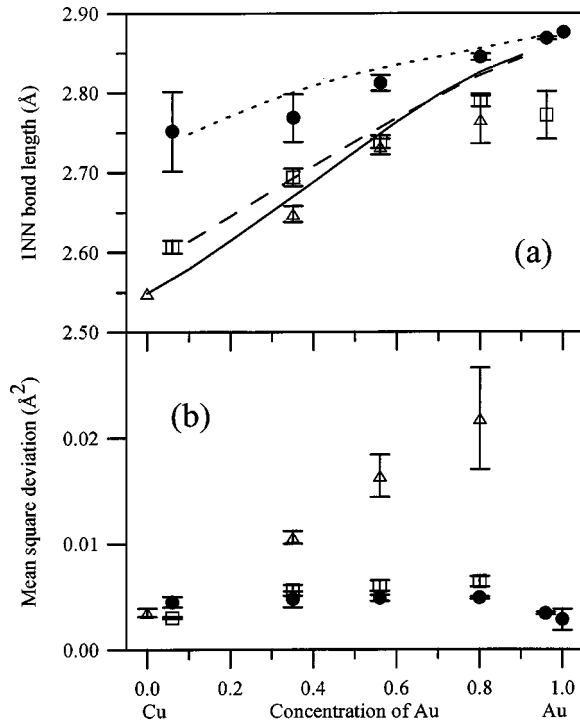| $x$ | Au-Au | Au-Ag | Ag-Ag |
|---|---|---|---|
| 0 | | | 0.0036(5) |
| 0.5 | 0.0026(5) | 0.0028(5) | 0.0038(5) |
| 1 | 0.0024(5) | | |

FIG. 4. (a) 1NN distances measured by XAFS at 80 K for Cu-Cu (triangles), Cu-Au (squares) and Au-Au (circles) atomic pairs. 1NN distances obtained from computer simulation are also presented for Cu-Cu (solid curve), Cu-Au (dashed curve), and Au-Au (dotted curve) pairs. (b) mean-square deviations $\sigma^2$ of the 1NN pair lengths at 80 K as obtained from XAFS for Cu-Cu (triangles), Cu-Au (squares), and Au-Au (circles) atomic pairs.

ent trend in the compositional dependence of the Au-Au, Au-Cu, and Cu-Cu bonds [Fig. 4(a)]. The short Cu-Cu bond length exhibits stronger variation with $x$ than the Au-Au bond length, i.e., the Cu-Cu bond expands easier with the increase of Au concentration than the Au-Au bond contracts when the concentration of Cu increases.

The qualitative interpretation of this effect is the following. From the asymmetry of the pair interaction potential (repulsive branch is steeper than the attraction branch) the compressed bond (Au-Au) is expected to be stiff relative to the expanded bond (Cu-Cu). The concomitant nonzero residual elastic strain energy, accumulated in the alloy system with the atomic size mismatch due to the distortion of each bond from its equilibrium length, determined by the pure metal, is larger for a system with stronger distortions of atoms from the periodic positions.[3] To increase the strain energy by the same amount requires less change (shortening) $\delta R_{Au}$ of the effective Au-Au bond than the change (elongation) $\delta R_{Cu}$ of the Cu-Cu bond because in the former case the elastic strain is stored in the stiffer ''spring.'' The increase of

the elastic energy is minimized when $\delta R_{Au}$ is smaller than $\delta R_{Cu}$.

To verify this intuitive argument (first-principles study by Ozolins, *et al.*[26] showed good qualitative agreement with our results), accurate local structure measurement is vital. We performed concurrent multiedge, multiple data set refinement of our XAFS data which allowed us to obtain interatomic distances with uncertainties as small as 0.002 Å. We calibrated the reliability and sensitivity of our procedure for the system of $Au_{0.5}Ag_{0.5}$ where no local structural distortions are expected in advance, based on virtually indistinguishable lattice parameters of pure Au and Ag metals. Indeed, we obtained that the interatomic distances between Au-Au, Au-Ag, and Ag-Ag pairs are the same within small experimental uncertainties, and the $\sigma^2$ of these bonds fall in between those of the pure metals. In addition, as another reliability check, we obtained the same short-range-order parameter of 10% between nearest neighbors as found by previously published x-ray diffuse scattering analyses. Successful testing of our procedure against a known system greatly increases the confidence in the results obtained for the $Au_xCu_{1-x}$ alloy analyzed in the same manner as the $Au_{0.5}Ag_{0.5}$ system.

We believe that the observed bond lengths asymmetry is an intrinsic property of all disordered alloys. Such an asymmetry reduces local elastic strain caused by the atomic size mismatch and/or difference between the effective force con-
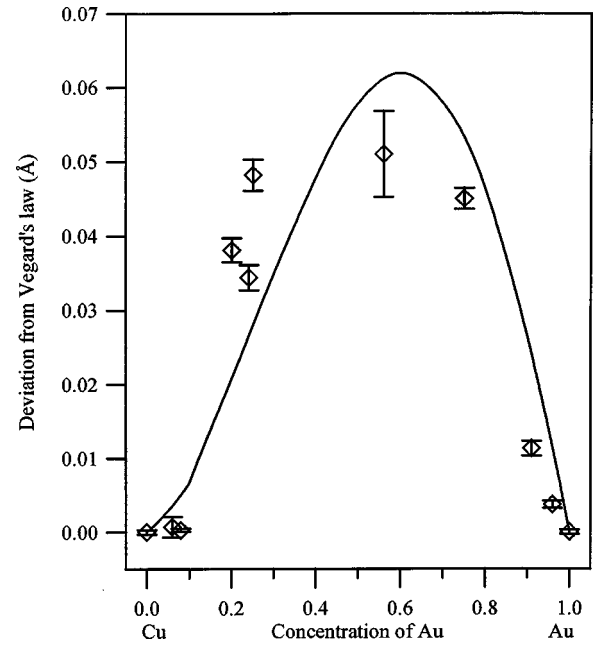


FIG. 5. The lattice parameter presented as deviation from the Vegard's law $a - a_0$ in $Au_xCu_{1-x}$ at 300 K as determined by x-ray diffraction (symbols) and from computer simulation (solid curve).

TABLE III. Static mean-square deviations (in $Å^2$) versus $x$ ($Au_xCu_{1-x}$) in 1NN pair lengths determined from XAFS data.

| $x$ | Au-Au | Au-Cu | Cu-Cu |
|------|-----------|-----------|------------|
| 0.35 | 0.0028(13) | 0.0029(7) | 0.0062(9) |
| 0.56 | 0.0030(4) | 0.0028(7) | 0.0104(30) |
| 0.80 | 0.0026(3) | 0.0035(10) | |

TABLE IV. Parameters of the potentials used in our simulation of $Au_xCu_{1-x}$ alloys.

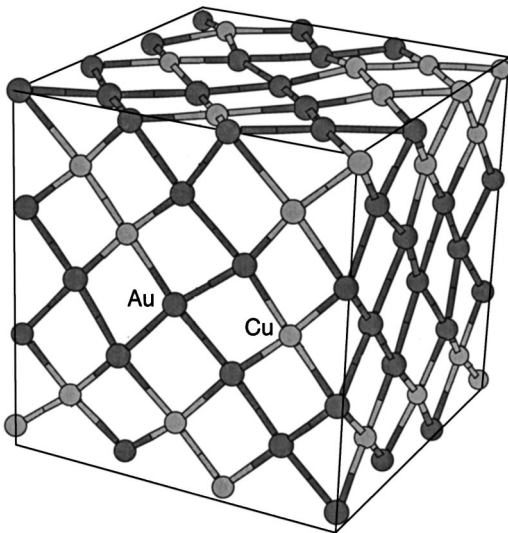| Bond $T'$-$T$ | $R_{T'T}$ (Å) | $K_{T'T}$ (eV/$Å^2$) |
|---------------|-----------------|------------------------|
| Cu-Cu | 2.549 | 2.29 |
| Au-Au | 2.876 | 3.10 |
| Cu-Au | 2.670 | 2.00 |

FIG. 6. The inner part ($3\times3\times3$ unit cells) of the $Au_{0.5}Cu_{0.5}$ cluster obtained from computer simulations. The deviations from the average fcc sites are magnified by a factor of 2 for better visualization. If there were no deviations, the bonds would all align along straight lines, including the edge atoms which would align along the cube lines.

stants between different pairs of atoms. The seeming contradiction in the experimental studies of different binary and pseudobinary alloys where such asymmetry was observed in some systems (e.g., RbBr-RbCl, RbBr-KBr, Au-Cu, Si-Ge) and not observed in many others, e.g., semiconductor III-V alloys, needs to be clarified. The requirement for the experimental detection of the bond lengths asymmetry is picking an alloy with strong compositional change of nearest-neighboring distance. The ''topological rigidity parameters'' introduced by Cai and Thorpe,[27] and characterizing the rigidity of the lattice system of the alloy are useful phenomenological figures of merit which are expected to be closer to the absolute rigidity limit of 1 for the semiconductor alloys than for the ionic or metallic alloys, due to the strongly directional covalent bonding between the atoms in semiconductors. Indeed, the distortion of the nearest-neighbor bond length did not exceed 20% of the atomic size difference in the pure GaAs and InAs in pseudobinary semiconductor alloys $Ga_xIn_{1-x}As$.[8] We believe that in these and other experiments with semiconductor alloys the sensitivity of XAFS measurement was not sufficient to detect the bond length asymmetry effects outside the uncertainties because they were so small. In the cases where these effects were observed[1–3] as well as in the present work, the interatomic bonds were ionic or metallic, i.e., less directional and relatively soft compared to those in semiconductor alloys. The most recent example[10] shows that similar effect was observed in the semiconductor binary alloy Si-Ge which was studied by the similar multiedge, multiple data set refinement as in our preliminary report[23] and in the present work. In the Si-Ge alloy, however, the rigidity parameters are relatively high [0.7 (Ref. 28)] which explains why the difference in the slopes of the Si-Si, Si-Ge, and Ge-Ge bond lengths is within the uncertainties of the measurements.

As just discussed, the difference in the scenarios of short and long bond length changes with concentration can be un-

derstood by the asymmetry in the pair potentials. However, in addition to this conclusion, obtained from the observed difference in the tendency of Au-Au and Cu-Cu bond lengths to change with concentration, a unique insight into local atomic arrangement in this alloy can be gained from the measurements of the Debye-Waller factors [Fig. 4(b)]. Consistent with a relatively small change with Au concentration of Au-Au bond length with respect to its value in pure Au, the $\sigma^2$ of this bond does not change strongly with $x$ either. A similar observation can be made from comparing the Au-Cu bond length and $\sigma^2$ changes with $x$. This is in contrast with the Cu-Cu bonds which have a drastic increase of $\sigma^2$ with $x$. Along with the observed larger slope of the $x$ dependence of Cu-Cu bond length than for other bonds, these results together all indicate that the small Cu atoms become loosened in the Au matrix at large enough $x$ ($x>0.35$), and the Cu-Cu 1NN pairs are losing contact, while Cu-Au and Au-Au 1NN pairs remain in contact at all concentrations.

Finally, it should be emphasized that the pair interactions as determined from XAFS measurements, with parameters listed in Table IV for the $Au_xCu_{1-x}$ alloys, are not the ''bare'' pair interactions calculated for isolated atoms as in a diatomic molecule. They are a ''dressed'' or renormalized one in the alloy determined by averaging over the positions of all other atoms in the alloy.[29] This effective interaction, which contains all many-body interactions, is also called in the literature the thermally averaged pair potential[29] and the potential of mean force.[30]

## VI. CONCLUSIONS

The detailed structure of the rapidly quenched $Au_xCu_{1-x}$ alloys was investigated by XAFS, XRD, and computer simulation. The atoms were found to be randomly disordered among the atomic sites which deviated locally from the average fcc crystal sites. The observed difference in distance change (Cu-Cu bond length changes more rapidly with Au concentration than Au-Au and Au-Cu bond lengths) can be understood by the asymmetry in the renormalized pair potentials where the repulsive forces are stronger than the attractive ones. The loosening of the contact in the Cu-Cu pairs with Au concentration was indicated by the anomalous increase of $\sigma^2$ of these bonds. The computer simulation on a cluster of $10^5$ atoms reproduces the main features of both our XAFS and XRD data and links the microscopic parameters obtained by XAFS with the macroscopic XRD measurement, while allowing a visualization of the local distortions from the average fcc lattice.

For comparison the disordered $Au_{0.5}Ag_{0.5}$ alloy was also investigated by XAFS and XRD, and its atoms were found to have insignificant deviations from an ideal fcc lattice. This different effect of alloying between metallic alloys is understood by the difference in perturbations introduced by the alloying. In the case of Au-Ag alloys, the perturbation is quite small, while in Au-Cu alloys, it is quite significant.

A discussion summarizing previously published works is also given on the difference of the distortions from the average periodic lattice in other chemically disordered materials, namely, covalent and ionic bonded ones. Whereas the decrease in bond distance between the larger atoms and the increase in bond distance between the smaller atoms in

covalent bonded materials varies symmetrically with composition, an asymmetric variation is evident in the ionic and metallic cases. This asymmetric variation is expected because pair interaction potentials generally have an asymmetry with a stronger repulsive force at shorter distances than the attractive force at larger distances. The lack of the observation of such an asymmetry in the covalent alloyed samples with more rigid bonds is believed to be due to the smaller change in bond distances, which makes the anharmonic nature of the pair interaction too small to be detected.

[1] A.I. Frenkel, E.A. Stern, A. Voronel, M. Qian, and M. Newville, Phys. Rev. Lett. **71**, 3485 (1993).

[2] A.I. Frenkel, E.A. Stern, A. Voronel, M. Qian, and M. Newville, Phys. Rev. B **49**, 11 662 (1994).

[3] A.I. Frenkel, E.A. Stern, A. Voronel, and S. Heald, Solid State Commun. **99**, 67 (1996).

[4] A.I. Frenkel, A. Voronel, A. Katzir, M. Newville, and E.A. Stern, Physica B **208&209**, 334 (1995).

[5] S.I. Zabinsky, J.J. Rehr, A. Ankudinov, R.C. Albers, and M.J. Eller, Phys. Rev. B **52**, 2995 (1995).

[6] E.A. Stern, M. Newville, B. Ravel, Y. Yacoby, and D. Haskel, Physica B **208&209**, 117 (1995). The UWXAFS software is licensed through the University of Washington.

[7] J.C. Woicik, Phys. Rev. B **57**, 6266 (1998); J.C. Woicik, J.G. Pellegrino, B. Steiner, K.E. Miyano, S.G. Bompadre, L.B. Sorensen, T.-L. Lee, and S. Khalid, Phys. Rev. Lett. **79**, 5026 (1997); J.C. Woicik, J.A. Gupta, S.P. Watkins, and E.D. Crozier, Appl. Phys. Lett. **73**, 1269 (1998).

[8] J.C. Mikkelson, Jr. and J.B. Boyce, Phys. Rev. Lett. **49**, 1412 (1982).

[9] J.C. Woicik, K.E. Miyano, C.A. King, R.W. Johnson, J.G. Pellegrino, T.-L. Lee, and Z.H. Lu, Phys. Rev. B **57**, 14 592 (1998).

[10] J.C. Aubry, T. Tyliszczak, A.P. Hitchcock, J.-M. Baribeau, and T.E. Jackman, Phys. Rev. B **59**, 12 872 (1999).

[11] K.E. Miyano, J.C. Woicik, L.H. Robins, C.E. Bouldin, and D.K. Wickenden, Appl. Phys. Lett. **70**, 2108 (1997); L. Bellaiche, S.-H. Wei, and A. Zunger, Phys. Rev. B **56**, 13 872 (1997).

[12] J. Langford and D. Louër, Rep. Prog. Phys. **59**, 131 (1996).

[13] E.A. Stern and K. Kim, Phys. Rev. B **23**, 3781 (1991).

[14] M. Newville, P. Livins, Y. Yacoby, J.J. Rehr, and E.A. Stern, Phys. Rev. B **47**, 14 126 (1993).

[15] E. A. Stern and S. M. Heald, in *Handbook on Synchrotron Radiation*, edited by E. E. Koch (North-Holland, New York, 1983), Vol. 1.

[16] D. C. Koningsberger and E. A. Stern (private communication).

[17] M.S. Nashner, A.I. Frenkel, D.L. Adler, J.R. Shapley, and R.G. Nuzzo, J. Am. Chem. Soc. **119**, 7760 (1997); G.H. Via, K.F. Drake, G. Meitzner, F.W. Lytle, and J.H. Sinfelt, Catal. Lett. **5**, 25 (1990).

[18] Au $L_3$-, Ag $K$-, and Cu $K$-edges XAFS data were provided courtesy of M. Newville.

[19] A.I. Frenkel and J.J. Rehr, Phys. Rev. B **48**, 585 (1993).

[20] S.V.N. Naidu and C.R. Houska, J. Appl. Phys. **42**, 4971 (1971).

[21] N. Norman and B.E. Warren, J. Appl. Phys. **22**, 483 (1951).

[22] B.L. Averbach, P.A. Flinn, and M. Cohen, Acta Metall. **2**, 92 (1954).

[23] A.I. Frenkel, E.A. Stern, A. Rubshtein, A. Voronel, and Yu. Rosenberg, J. Phys. IV **7**, C2-1005 (1997).

[24] O. Malis, K.F. Ludwig, D.L. Olmsted, and B. Chakraborty, Philos. Mag. B **79**, 869 (1999).

[25] V. Ozolins, C. Wolverton, and A. Zunger, Phys. Rev. B **58**, R5897 (1998).

[26] V. Ozolins, C. Wolverton, and A. Zunger, Phys. Rev. B **57**, R6427 (1998).

[27] Y. Cai and M.F. Thorpe, Phys. Rev. B **46**, 15 879 (1992).

[28] N. Mousseau and M.F. Thorpe, Phys. Rev. B **46**, 15 887 (1992).

[29] E.A. Stern, *Proceedings of the 9th International Conference on X-ray Absorption Fine Structure* [J. Phys. IV **7**, C2-137 (1997)].

[30] N. E. Cusak, *The Physics of Structurally Disordered Matter: An Introduction* (Adam Hilger: University of Sussex Press, Bristol, UK, 1987).